Mechanically Strong and Multifunctional Polyimide Nanocomposites Using Amimophenyl Functionalized Graphene Nanosheets

ARTICLE *in* MACROMOLECULES · MAY 2013

Impact Factor: 5.8 · DOI: 10.1021/ma400185j

6 AUTHORS, INCLUDING:

Joong Hee Lee
Chonbuk National University
240 PUBLICATIONS **6,058** CITATIONS
SEE PROFILE

Bon-Cheol Ku
Korea Institute of Science and Technology, Ins…
67 PUBLICATIONS **931** CITATIONS
SEE PROFILE

Macromolecules

Article

pubs.acs.org/Macromolecules

Mechanically Strong and Multifunctional Polyimide Nanocomposites Using Amimophenyl Functionalized Graphene Nanosheets

Ok-Kyung Park,[†,§] Jun-Yeon Hwang,[†] Munju Goh,[†] Joong Hee Lee,[§] Bon-Cheol Ku,[†,*] and Nam-Ho You[†,*]

[†]Carbon Convergence Materials Research Center, Institute of Advanced Composites Materials, Korea Institute of Science and Technology, Eunha-ri san 101, Bondong-eup, Wanju-gun, Jeollabuk-do, 565-905, Korea

[§]Department of BIN Fusion Technology and Department of Polymer and Nano Science and Technology, Chonbuk National University, Duckjin-dong 1Ga, 64-14, Jeonju, Jeollabuk-do, 561-756, Korea

Supporting Information

ABSTRACT: We report an effective way to fabricate mechanically strong and multifunctional polyimide (PI) nanocomposites using aminophenyl functionalized graphene nanosheet (APGNS). APGNS was successfully obtained through a diazonium salt reaction. PI composites with different loading of APGNS were prepared by *in situ* polymerization. Both the mechanical and electrical properties of the APGNS/PI composites were significantly improved compared with those of pure PI due to the homogeneous dispersion of APGNS and the strong interfacial covalent bonds between APGNS and the PI matrix. The electrical conductivity of APGNS/PI (3:97 w/w) was 6.6×10^{-2} S/m which was about 10^{11} times higher than that of pure PI. Furthermore, the modulus of APGNS/PI was increased up to 16.5 GPa, which is approximately a 610% enhancement compared to that of pure PI, and tensile strength was increased from 75 to 138 MPa. The water vapor transmission rate of APGNS/PI composites (3:97 w/w) was reduced by about 74% compared to that of pure PI.

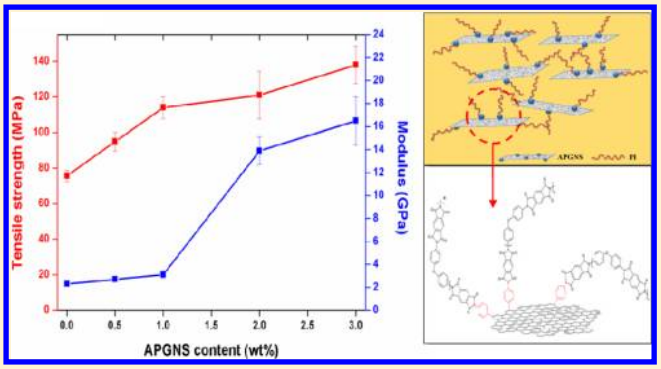

INTRODUCTION

Aromatic polyimide (PI) is a high-performance polymer with applications in the fields of microelectronics, optoelectronics, adhesives, and aerospace owing to its high thermal stability and favorable chemical and mechanical properties.[1,2] However, PI has a few limitations, such as electrostatic accumulation, poor heat dissipation, and low electrical conductivity for special applications. In recent years, much attention has been paid to PI composites with carbon nanomaterials because the incorporation of carbon nanofillers can effectively enhance the thermal, mechanical, and electrical properties of the nanocomposites.[2−6]

Graphene, a one-atom-thick planar sheet of carbon atoms densely packed in a honeycomb crystal lattice,[7] has revolutionized the scientific frontiers of nanoscience and condensed matter physics due to its exceptional electrical,[8] physical,[9] and chemical properties.[10] The excellent properties of graphene have opened new pathways for developing a wide range of novel functional materials. In addition, graphene has a distinctive mechanical property with fracture strains of ∼25% and a Young's modulus of ∼1 TPa.[9] However, poor dispersion in organic solvents and weak interfacial interactions between graphene and the polymer matrix limit the widespread use of graphene. In contrast, graphene oxide (GO) produced by the oxidation of graphite can solve these issues. It is easily dispersed in water and polar solvents due to the functional groups, such as ketones, diols, epoxides, hydroxyls, and carbonyl, on its edges and basal planes.[11] Nevertheless, GO has limited compatibility with certain polymers and limited solubility in hydrophobic solvent owing to its hydrophilic nature, which can reduce the reinforcement effects of interfacial interaction in the polymer matrix.[12,13]

Therefore, the key issue is to improve both the homogeneous dispersion and strong interfacial interaction between the polymer matrix and graphene for the development of high performance polymer/graphene nanocomposites. Recently, many researchers have developed surface functionalized graphene oxide as a filler to improve compatibility between the PI matrix and graphene, enhancing the mechanical properties of composite materials via *in situ* polymerization.[2,5]

Although the compatibility and mechanical properties of PI composite materials were improved by using modified GO, the electrical properties did not increase significantly.[2] This is because electrical conductivity depends on the intrinsic filler properties. The intrinsic electrical conductivity of graphene depends on the degree of surface functionalization of graphene.

Received: January 28, 2013
Revised: March 27, 2013
Published: April 15, 2013

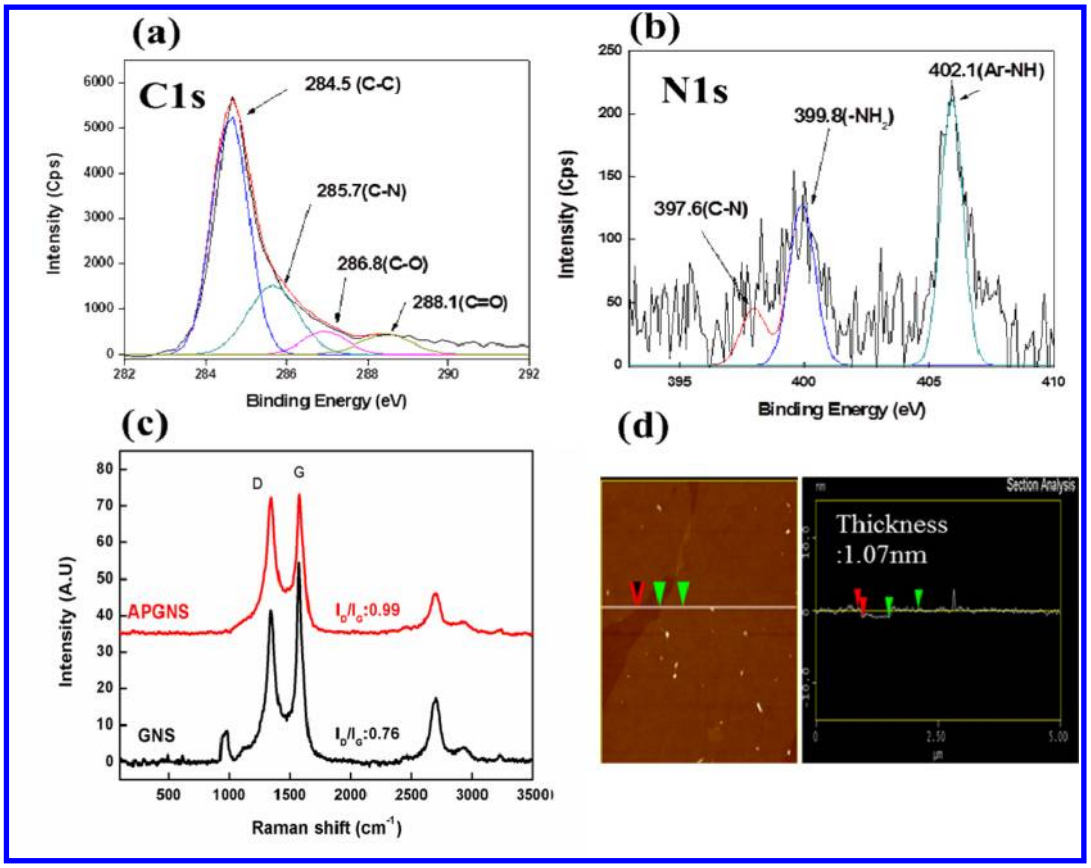

Figure 1. XPS C1s (a) and N1s (b) spectra of the APGNS for experimental XPS survey spectra and deconvoluted peaks, (c) Raman spectra and I_D/I_G ratio of GNS and APGNS, and (d) typical tapping mode AFM image and thickness of APGNS after homogenization for 1 h in NMP solvent.

In particular, the intrinsic electrical conductivity of graphene corresponds to the number of defects that can be found on its surface. These defects are usually generated during the oxidation–reduction process of graphene.[14,15]

Chemically modified graphene which can induced chemical bonding between PI matrix and graphene to improve both electrical and mechanical properties.[5,16]

However, these polymer composites were prepared by being mixed mechanically with chemically modified graphene and extruded by a hot press method, which was not effective for introducing highly dispersed graphene into the polymer matrix.

In this study, we will demonstrate an effective method for preparing aminophenyl functionalized graphene nanosheets (APGNS)/PI composite materials via *in situ* polymerization for high performance nanocomposites. APGNS was synthesized by a diazonium salt reaction using thermally reduced graphene nanosheet (GNS). This method can minimize defects in the GNS.

APGNS can not only improve homogeneous dispersion in a polar solvent but also enhance mechanical properties while maintaining high electrical conductivity, owing to covalent bonding between the PI matrix and the GNS. Moreover, a low imidization temperature using a base catalyst such as 1,4-diazobicyclo[2.2.2]octane (DABCO) and 1,8-diazabicyclo[5.4.0]undec-7-ene (DBU) to prepare composite films effectively improved mechanical properties, which can reduce the elimination of functional groups on GNS at high temperatures.[17,18] We also demonstrated that the water vapor permeability of composite films decreased significantly by 74% compared to that of pure PI.

EXPERIMENTAL SECTION

Materials. Commercial graphene nanosheet (GNS, grade C; surface area, 300m^2/g; average thickness, ~2 nm; average diameter, <2 μm) was provided by XG sciences (USA). The thermally reduced GNS was obtained after heating at 1500 °C for 1 h. Concentrated sulfuric acid, methanol and *N*,*N*′-dimethlyformamide (DMF) were purchased from Samchun Chemicals (Korea). Nitrobenzene diazonium-tetrafluoroborates, phosphoric acid and ammonium hydroxide were purchased from Sigma-Aldrich (USA). The poly(amic acid) (PAA) was prepared via *in situ* polymerization. Pyromellitic dianhydride (PMDA), 4, 4-oxidianiline (ODA), and 1-methyl-2-pyrolidinone (NMP) were purchased from Sigma-Aldrich (USA). Finally, 1,4-Diazabicyclo[2,2,2]octane (DABCO) was purchased from TCI (Japan). All chemicals were used as received without further purification.

Preparation of Aminophenyl-Functionalized Graphene Nanosheet (APGNS). Thermally reduced GNS (0.1 g) was immersed in H_2SO_4 (100 mL), undergoing sonication for 30 min, followed by the addition of 1.8 g of nitrobenzene diazonium-tetrafluoroborates. The mixture was magnetically stirred vigorously at 60 °C for 1 h. After cooling to room temperature, the mixture was diluted and washed with DMF. Finally, the product was washed with ethanol and dried at 60 °C for 24 h in a vacuum oven to get the nitrophenyl functionalized graphene nanosheet (NPGNS). Then, 0.1 g of dried NPGNS was added to a solution of phosphoric acid (45 g) and DI-water (50 mL). The mixture was stirred at 115 °C for 6 h. After cooling to room temperature, the reactant mixture was transferred into a mixed solution of 200 mL of ammonium hydroxide and 100 mL of methanol.

Then, the mixture was diluted with DI-water and stirred for 6 h for desalination. The APGNS was washed with ethanol and dried at 60 °C for 24 h in a vacuum oven.

Preparation of APGNS/PI Composites via *in Situ* Polymerization. Neat PI and APGNS/PI films were prepared through the

dx.doi.org/10.1021/ma400185j | *Macromolecules* 2013, 46, 3505–3511

conventional two-step procedure: poly(amic acid) (PAA) precursors followed by thermal imidization at elevated temperatures.

APGNS and DABCO (0.021g, 0.18 mmol) were immersed in NMP (11.8 g). After sonication of the mixture for 1 h at room temperature, ODA (1g, 5 mmol) was added to it. The APGNS and diamine mixture were stirred for 1 h before the PMDA was added. The ODA was completely dissolved in the NMP. PMDA (1.1 g, 5 mmol) was then added to the mixture, which was stirred overnight at room temperature. The prepared mixture of APGNS and PAA was casted on the PI film using a doctor blade. The cast film was first dried in a vacuum oven at 80 °C for 3 h to remove the residual solvent. APGNS/PI composite films were prepared with the thermal curing of the PAA in an oven for 1 h, with steps of 80, 150, and 30 min at 200 °C.

Characterization. The thickness of the APGNS after homogenization was measured by using atomic force microscopy (AFM) (Nanoscope IIIa-Multimode AFM, Veeco-Digital Instruments, USA). The AFM samples were prepared by depositing the homogeneous APGNS mixture onto a silicon substrate in an NMP solution (0.1 mg/mL).

The introduction of chemical bonds and functional groups onto the graphene surface was confirmed by XPS (X-ray photoelectron microscopy, AXIS-NOVA, Kratos Inc., USA) and Raman spectroscopy (LabRAM HR, Horiba, Japan).

Thermogravimetric analyses (TGA) were carried out with a TA 50 (TA Instruments, USA) under nitrogen gas flow at a heating rate of 5 °C/min.

Samples were prepared by first dispersing the GNS/APGNS in deionized water. Then, the dispersion was dropped on a carbon grid and air-dried before observation. The electrical conductivity of the APGNS/PI composites was measured using a 4-point probe method (FPP-RS8, Dasol Eng, Korea).

The tensile strength and modulus of the APGNS/PI composites were also measured on a universal testing machine (UTM, 5567A, Instron, USA). Twenty specimens with lengths of 25 mm and widths of 5 mm were prepared for each tensile test. The speed of the crosshead was 1 mm/min.

The barrier properties of APGNS/PI composites were also examined. The water vapor permeability of pure PI and APGNS/PI composites were measured using a water vapor transmission analyzer (AQUATRAN Model 1, Mocon, USA).

The cross-section of the fractured tensile specimen was analyzed using scanning electron microscopy (SEM: S-4700, Hitachi, Japan). To observe the microstructures of GNS and APGNS, a JEM-2200FS (JEOL, Japan) transmission electron microscope (TEM) was used at 200 kV. For the TEM sample preparation, the GNS and APGNS were dispersed in deionized water, and subsequently the dispersion was dropped on a carbon grid and air-dried. During the TEM study, the exposal time of the accelerated electrons was minimized to avoid electron radiation damage.

RESULT AND DISCUSSION

Characterization of APGNS. The APGNS was investigated by Raman spectroscopy, XPS, and TGA analysis. Parts a and b of Figure 1 showed the spectra of the XPS C1s and N1s original and fitted curves. The C 1s spectra of APGNS were fitted to identify the changes in surface chemistry. APGNS showed four peaks at 284.5, 285.7, 286.7, and 288.1 eV, corresponding to C−C, C−N, C−O, and C═O groups, respectively.[19] N1s also showed three peaks at 397.6, 399.8, and 402.1 eV, corresponding to C−N, $-NH_2$, and Ar$-NH_2$, respectively.[19−21] The localization of electrons initiated the formation of Ar$-NH_2$ covalent bonding, which generally appeared at 402.1 eV. This clearly conformed to the presence of Ar$-NH_2$ groups on the surface of graphene via diazonium salt reaction. The calculated atomic ratios of the constituent element in the APGNS based on XPS was listed in Table S1, Supporting Information. The calculated atomic ratios of the constituent elements in the APGNS based on high-resolution

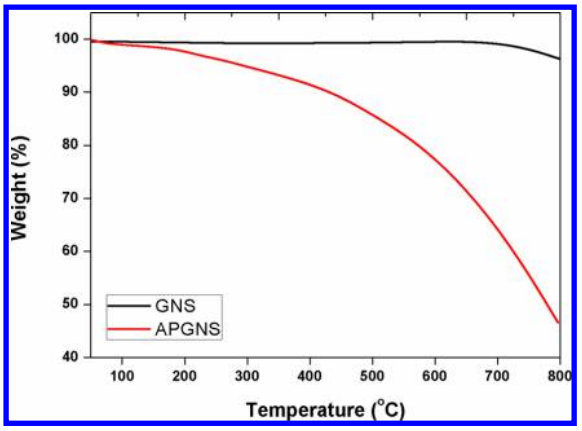

Figure 2. TGA thermogram of GNS and APGNS. (N_2 atmosphere, heating rate = 5 °C/min).

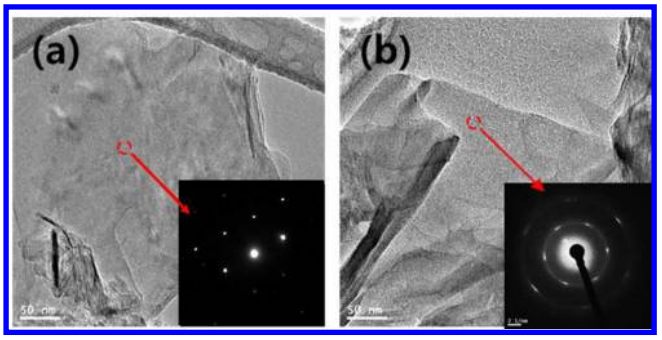

Figure 3. TEM and SAD images: (a) GNS and (b) APGNS.

Table 1. Mechanical and Electrical Properties of Pure PI and APGNS/PI Composites

sample	tensile strength (MPa)	modulus (GPa)	elongation (%)	electrical conductivity (S/m)
pure PI	75.7 ± 3.1	2.3 ± 0.15	18.5 ± 4.2	1.2×10^{-13}
APGNS/PI (0.5:99.5)	95 ± 5.2	2.7 ± 0.21	15.2 ± 3.1	4.2×10^{-6}
APGNS/PI (1:99)	114 ± 6.1	3.0 ± 0.3	16.9 ± 2.1	8.6×10^{-5}
APGNS/PI (2:98)	121 ± 13.4	13.9 ± 1.2	7.4 ± 2.1	9.2×10^{-4}
APGNS/PI (3:97)	138 ± 10.6	16.5 ± 2.1	8.7 ± 1.8	6.6×10^{-2}

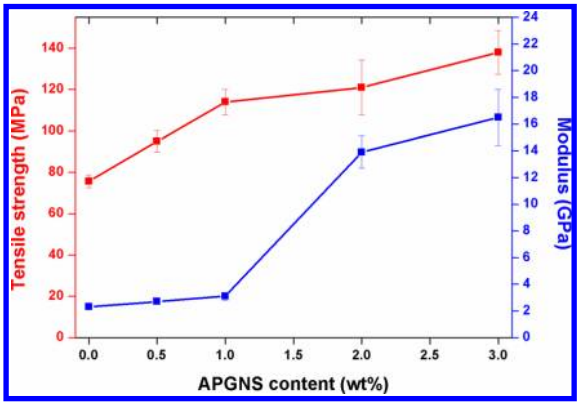

Figure 4. Mechanical properties of increasing amounts of APGNS incorporated into PI composites (APGNS/PI).

dx.doi.org/10.1021/ma400185j | Macromolecules 2013, 46, 3505−3511

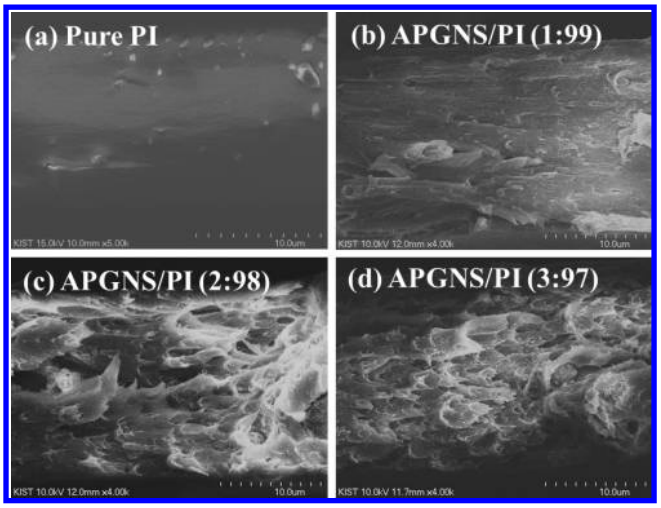

Figure 5. SEM images of fracture surface of pure PI and its nanocomposites containing various amounts of APGNS: (a) pure PI, (b)1 wt % APGNS/PI, (c) 2 wt % APGNS/PI, and (d) 3 wt % APGNS/PI composites.

of XPS was 90.59% (C1s), 6.79% (O1s), 2.29% (N1s), and 0.33% (S 2p). The atomic ratio of the nitrogen was introduced due to aminophenyl functionalization, indicating that the APGNS can be successfully functionalized by diazonium salt reaction.

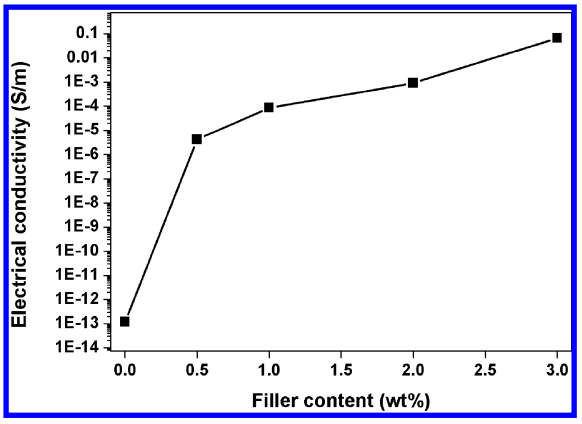

Figure 7. Electrical conductivity of APGNS-incorporated PI composites (APGNS/PI) with increasing amounts of APGNS.

Figure 1c showed the Raman spectra of the APGNS. The Raman spectrum of the APGNS showed two strong bands: the G-band at around 1580 cm^{-1} and the D-band at around 1350 cm^{-1}.

The G-band was due to the first order scattering of the E_{2g} phonon of sp^2 carbon and the D-band arises from a defect in

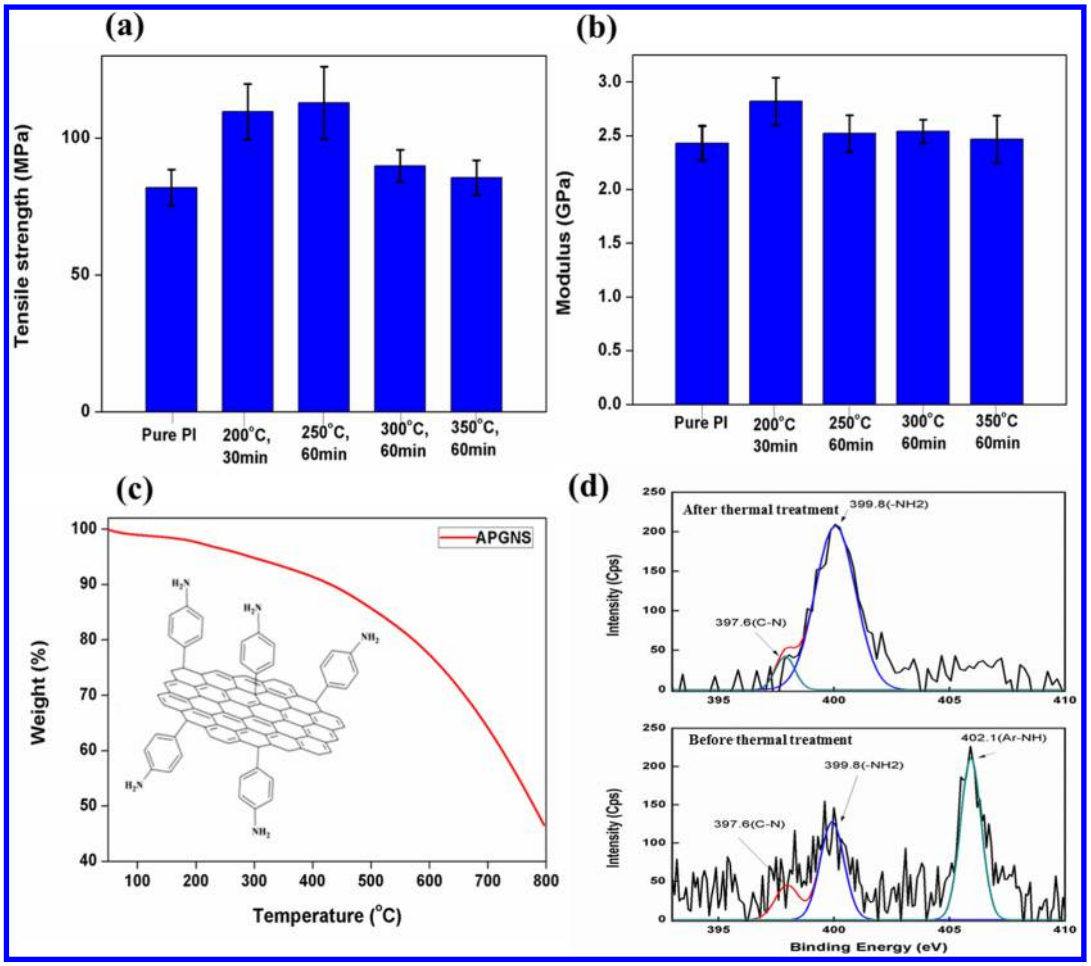

Figure 6. Tensile strength (a) and modulus (b) of 1 wt % APGNS incorporated PI composites at various imidization temperatures, (c) TGA thermogram of APGNS (heating rate: 5 °C/min under nitrogen), and (d) XPS N 1s spectra before and after thermal treatment (300 °C, 1 h, air conditioning) of APGNS.

dx.doi.org/10.1021/ma400185j | *Macromolecules* 2013, 46, 3505−3511

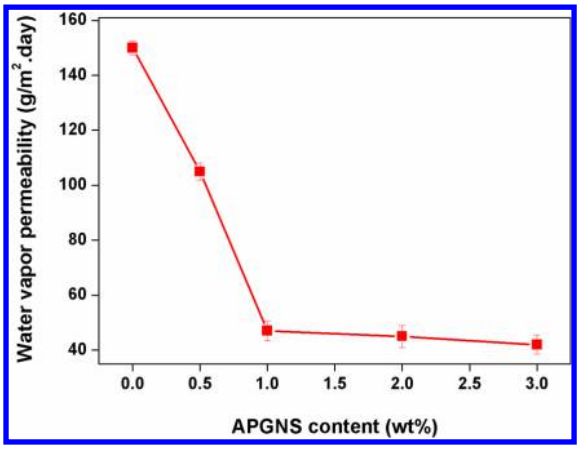

Figure 8. Water vapor permeability of APGNS-incorporated PI composites (APGNS/PI) with increasing amounts of APGNS.

the carbon structure.[22,23] Therefore, the ratio of intensity from the D-band to the G-band (I_D/I_G) corresponded to the amount of sp^3-hybridized carbon atoms in the sp^2 conjugated graphene, and thus provides direct evidence of the degree of functionalization.[24] The ratio of I_D/I_G of APGNS was increased from 0.76 to 0.99 after aminophenyl functionalization.

This clearly indicates that the aminophenyl functional group was covalently bonded on the surface of the graphene after surface functionalization.

Atomic force microscopy (AFM) was used to quantify the degree of exfoliation of graphene sheet. The AFM image (Figure 1d) of APGNS after homonization for 1 h in NMP showed that APGNS with thickness of 1.07 nm was obtained. It should be noted that the thickness of APGNS was higher than that of graphene (0.3 nm),[25] which can be attributed to the grafting of aminophenyl functional groups on the surface of graphene.[26−28] This result indicated a successful exfoliation of APGNS in the NMP solution.

TGA thermograms (Figure 2) of the GNS and APGNS showed the functional groups on the graphene surface. The first weight loss of APGNS at around 100 °C was considered to be probably due to the evaporation of moisture. The second weight loss between 100 and 500 °C was attributed to the degradation of aminophenyl functional groups and remaining oxegen functional groups on the graphene surface.[29] The third weight loss between 500 and 800 °C was due to the decomposition of the carbon structure. The results indicated that aminophenyl groups on the graphene surface were successfully introduced via diazonium salt reaction. The microstructure obtained from TEM and selected area diffraction (SAD) patterns in an inset taken from GNS and APGNS are shown in Figure 3. The two samples showed the typical morphology of graphene.

The SAD pattern revealed that the GNS sample clearly represented the normal pattern of graphite or multilayered graphite shown in Figure 3a. The SAD pattern obtained from APGNS sample in Figure 3b showed the diffused rings along the {1100} planes, evidence that multiple graphene sheets have continuous hexagonal symmetry. From these nanostructures, the whole process was well established without the loss of GNS and APGNS characteristics.

Mechanical Properties of APGNS/PI Composites. Given the existence of covalent bonding between the graphene and PI at the interface and the homogeneous dispersion of graphene in the PI matrix, one would expect a substantial enhancement in the mechanical properties of the resulting composite.[30] The mechanical properties of pure PI and APGNS/PI composites with various loadings of APGNS were measured, and the typical stress−strain curves were shown in Figure S3, Supporting Information.

The tensile strength and modulus of these samples were summarized in Table 1. The relationships of mechanical properties with APGNS loading were illustrated in Figure 4. The APGNS/PI composites showed higher tensile modulus and strength compared to those of pure PI. In addition, both tensile strength and modulus of APGNS/PI composites were increased with an increase in APGNS contents (Figure 4). The modulus of the APGNS/PI composites with 3 wt % of APGNS increased by 617% from 2.3 to 16.5 GPa as compared to that of pure PI. In addition, the tensile strength of the APGNS/PI composites was increased from 75 to 138 MPa, which is a roughly 83% increase compared to that of pure PI. Such superior mechanical properties can certainly be attributed to the strong interfacial adhesion and good compatibility between the APGNS and the PI matrix.[30,5,6] Aminophenyl functional groups on the graphene surface can react with PMDA to form PAA, the intermediate state of PI. It could produce a strong chemical bond between the graphene and PAA. It was believed that the load can be transferred successfully from the PI matrix to the APGNS in a APGNS/PI composites.[30,5,6] Thus, the mechanical properties of the APGNS/PI composites were dependent upon the extent of the chemical bonding between the two phases. In addition, it was estimated that the APGNS can act as an effective reinforcement to improve the mechanical properties of the PI composites.

To confirm interfacial interaction between APGNS and the PI matrix, the fractured surfaces of APGNS/PI composites were observed by SEM upon tensile testing, as shown in Figure 5. The fractured surface of the pure PI was rather flat and smooth. For the PI nanocomposites containing APGNS, the fractured surface was comparatively rough. The rough fracture surface can be attributed to the strong interfacial interaction between APGNS and the PI matrix. It should be noted that the APGNS interlinked with the PI through chemical bonding, enhancing the mechanical properties of the PI composites.

Figure 6 showed the effects of imidization temperature on the mechanical properties of the APGNS/PI composites. The imidization temperature for the PI was charged from 200 to 350 °C and the mechanical properties of the APGNS/PI composites at various imidization temperatures were investigated. The results in parts a and b of Figure 6 suggested that the imidization temperature strongly affects the mechanical properties of the resulting PI composites. Among them, the PI composite prepared by heat treatment at 250 °C showed the highest tensile strength compared to others. However, the tensile strength of the APGNS/PI composite prepared at 300 °C decreased owing to the phase separation between the graphene and the PI matrix and the decomposition of functional groups on the graphene surface (Figure 6c).[31]

Defects in the nanostructured composites can reduce the reinforcement effects of graphene.[5] Figure 6d showed the XPS N 1s spectra before and after thermal treatment (300 °C for 1 h) of APGNS under air atmosphere. The N 1s of APGNS before thermal treatment showed characterization peaks at 397.6, 399.8, and 402.1 eV, corresponding to C−N, $-NH_2$, and $Ar-NH_2$, respectively.[19−21,32] After thermal treatment, the XPS spectrum did not show the $Ar-NH_2$ peaks due to the removal of functional groups during the thermal imidization process.

dx.doi.org/10.1021/ma400185j | *Macromolecules* 2013, 46, 3505−3511

Scheme 1. Schematic Diagram of Aminophenyl Functionalized Graphene Nanosheet (APGNS)

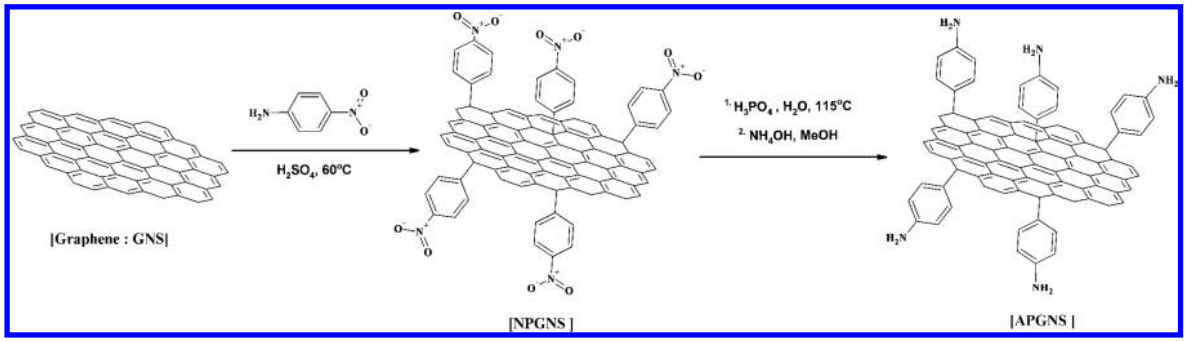

Scheme 2. *In Situ* Polymerization Pathway of APGNS-Incorporated PI Composites (APGNS/PI)

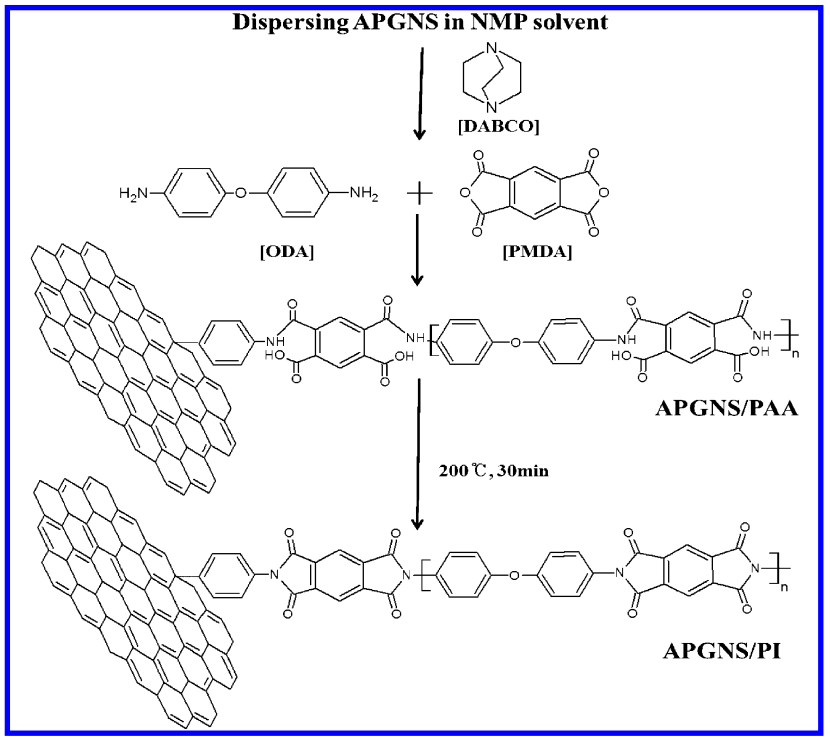

These results clearly confirmed that the aminophenyl functional groups on the surface of graphene decompose thermally at 300 °C,[31] resulting in the decrease of the mechanical properties of the composites probably due to the poor interaction/adhesion between graphene and the PI matrix.

Electrical Conductivity of APGNS/PI Composites. Graphene was reported to show excellent electron charge mobility of about 200 000 $cm^2/(V\ s)$ at room temperature,[33] and excellent electrical conductivity ($\sim 10^{-6}\Omega$ cm resistivity).[34] Consequently, graphene provides a percolated pathway for electron transfer; it can improve the electrical conductivity of the resulting composites. Figure 7 showed that the electrical conductivity of APGNS/PI increased with an increase in filler content. The electrical conductivity of the APGNS/PI composites increased sharply with increasing filler content up to 1 wt %. Above this content, it increased smoothly with increasing filler content. This can be attributed to the formation of a conductive network through the PI matrix.

The aminophenyl functional groups on the surface of the APGNS/PI composites can form amide groups with the PI during *in situ* polymerization, which enhances the dispersion and interfacial interaction between the graphene and the PI matrix. This result suggested that the loose network formation and improved dispersion of APGNS in the PI matrix through *in situ* polymerization can achieve an effective conductive pathway.[35−37] It could enhance the electrical conductivity of APGNS/PI composites compared to that of pure PI.

Water Vapor Permeability of APGNS/PI Composites. Combining graphene with the polymer matrix made it possible to produce barrier composite films. The 2D structure of graphene can improve the barrier properties of the polymer matrix if it lies in plane direction, according to the "tortuous path" model.[38−40] Herein, we investigated the water vapor permeability of pure PI APGNS/PI composites. Figure 8 showed that the water vapor permeability of the APGNS (1 wt %)/PI composite was decreased by about 74% compared to that of pure PI. The significant decrease in water vapor permeability was also considered to be presumably the homogeneous dispersion and highly exfoliated nanostructure of hydrophobic APGNS in the PI matrix,[41] increasing the tortuosity of the path of the water vapor molecules in the nanocomposites.[38] Therefore, APGNS/PI composite films can improve the water vapor barrier properties compared to pure PI.

dx.doi.org/10.1021/ma400185j | *Macromolecules* 2013, 46, 3505−3511

CONCLUSION

In summary, we designed and synthesized aminophenyl functionalized graphene nanosheet (APGNS) by a diazonium salt reaction using thermally reduced graphene nanosheet (GNS) to improve mechanical properties and electrical conductivity. The APGNS/PI composites showed a 83% increase in tensile strength, and 610% improvement in modulus with a low content of graphene nanosheets (~3 wt %) probably due to strong interfacial strength of graphene with PI matrix. Furthermore, water vapor permeability of APGNS/PI composites was also significantly reduced due to hydrophobic 2D structured graphene and the electrical conductivity of the PI composites containing 1 wt % APGNS increased 11-fold compared to that of pure PI. These results clearly show that the highly exfoliated functionalized graphene with strong interfacial strength with PI matrix is considered to provide an simple and effective way to develop ultrastrong and multifunctional polymer based nanocomposites with a wide range of applications.

ASSOCIATED CONTENT

Supporting Information

Information on characterization and instruments, XRD, TEM, SAD, atomic percentage of APGNS, the typical stress−strain curves of APGNS/PI composites, thermal stability, and the degree of imidization of APGNS/PI. This material is available free of charge via the Internet at http://pubs.acs.org.

AUTHOR INFORMATION

Corresponding Author

*Telephone: 82-63-219-8140. Fax: 82-63-219-8259. E-mail: polymer@kist.re.kr (N.-H.Y.) or cnt@kist.re.kr (B.-C.K.).

Notes

The authors declare no competing financial interest.

ACKNOWLEDGMENTS

This work was supported by a grant from the Korea Institute of Science and Technology (KIST) Institutional Program and the Converging Research Center Program funded by the Ministry of Education, Science and Technology (2012K001429) and the Fundamental R&D Program for Core Technology of Materials funded bythe Ministry of Knowledge Economy, Republic of Korea.

REFERENCES

(1) Kim, G. Y.; Choi, M.-C.; Lee, D.; Ha, C.-S. *Macromol. Mater. Eng.* **2012**, *297*, 303−311.
(2) Luong, N. D.; Hippi, U.; Korhonen, J. T.; Soininen, A. J.; Ruokolainen, J.; Johansson, L.-S.; Nam, J.-D.; Sinh, L. H.; Seppälä, J. *Polymer* **2011**, *52*, 5237−5242.
(3) Zhu, B.-K.; Xie, S.-H.; Xu, Z.-K.; Xu, Y. Y. *Compos. Sci. Technol.* **2006**, *66*, 548−554.
(4) Xiaowen, J.; Yuezhen, B.; Masaru, M. *Polymer* **2005**, *46*, 7418−7424.
(5) Wang, J.-Y.; Yang, S.-Y.; Huang, Y.-L.; Tien, H.-W.; Chin, W.-K.; Ma, C.-C. M. *J. Mater. Chem.* **2011**, *21*, 13569−13575.
(6) Ha, H. W.; Choudhury, A.; Kamal, T.; Kim, D.-H.; Park, S.-Y. *ACS Appl. Mater. Interfaces* **2012**, *4*, 4623−4630.
(7) Rao, C. N. R.; Sood, A. K.; Subrahmanyam, K. S.; Govindaraj, A. *Angew. Chem., Int. Ed.* **2009**, *48*, 7752−7777.
(8) Lee, C.; Wei, X. D.; Kysar, J. W.; Hone, J. *Science* **2008**, *321*, 385−388.
(9) Balandin, A. A. *Nat. Mater.* **2011**, *10*, 569−581.
(10) Dutta, S.; Pati, S. K. *J. Mater. Chem.* **2010**, *20*, 8207−8223.
(11) Dreyer, D. R.; Park, S.; Bielawski, C. W.; Ruoff, R. S. *Chem. Soc. Rev.* **2010**, *39*, 228−240.
(12) Pinto, A. M.; Cabral, J.; Tanaka, D. A. P.; Mendes, A. M.; Magalhaes, F. D. *Polym. Int.* **2013**, *62*, 33−40.
(13) Gao, Y.; Liu, L.-Q.; Zu, S.-Z.; Peng, K.; Zhou, D.; Han, B.-H.; Zhang, Z. *ACS Nano* **2011**, *5*, 2134−2141.
(14) Shin, H.- J.; Kim, K. K.; Benayard, A.; Yoon, S.-M.; Park, H. K.; Jung, I.-S.; Jin, M.-H.; Jeong, H.-K.; Kim, J. M.; Choi, J.-Y.; Lee, Y. H. *Adv. Funct. Mater.* **2009**, *19*, 1987−1992.
(15) Compton, O. C.; Dikin, D. A.; Putz, K. W.; Brinson, L. C.; Nguyen, S. T. *Adv. Mater.* **2010**, *22*, 892−896.
(16) Huang, H.; Lu, R.; Su, Chao.; Wang, H.; Guo, Z.; Liu, P.; Huang, Z.; Chen, H.; Li, T. *ACS Appl. Mater. Interfaces* **2012**, *4*, 2699−2708.
(17) Fukukawa, K.-I.; Shibasaki, Y.; Ueda, M. *Chem. Lett.* **2004**, *33*, 1156−1157.
(18) Devlin, C. L. H.; Chiang, S.; Russell, T. P. *J. Appl. Polym. Sci.* **2004**, *93*, 1192−1197.
(19) Lai, L.; Chen, L.; Zhan, D.; Sun, L.; Liu, J.; Lim, S. H.; Poh, C. K.; Shen, Z.; Lin, J. *Carbon* **2011**, *49*, 3250−3257.
(20) Lai, L. F.; Huang, G. M.; Wang, X. F.; Weng, J. *Carbon* **2010**, *48*, 3145−3156.
(21) Gromov, A.; Dittmer, S.; Svensson, J.; Nerushev, O. A.; Perez-Garcia, S. A.; Licea-Jimenez, L. *J. Mater. Chem.* **2005**, *15*, 3334−3339.
(22) Malard, L. M.; Pimenta, M. A.; Dresselhau, G.; Dresselhaus, M. S. *Phys. Rep.* **2009**, *473*, 51−87.
(23) Wang, Y. Y.; Ni, Z. H.; Yu, T.; Shen, Z. X.; Wang, H. M.; Wu, Y. H.; Chen, W.; Wee, A. T. S. *J. Phys. Chem. C.* **2008**, *112*, 10637−10640.
(24) Park, O.-K.; Lee, S.; Joh, H.-I.; Kim, J. K.; Kang, P.-H.; Lee, J. H.; Ku, B.-C. *Polymer* **2012**, *53*, 2168−2174.
(25) Gupta, A.; Chen, G.; Joshi, P.; Tadigadapa, S.; Eklund, P. C. *Nano Lett.* **2006**, *6*, 2667−2673.
(26) Stankovich, S.; Pine, R. D.; Nguyen, S. B. T.; Ruoff, R. S. *Carbon* **2006**, *44*, 3342−3347.
(27) Heyong, H.; Klinowski, J.; Forster, M.; Lerf, A. *Chem. Phys. Lett.* **1998**, *287*, 53−56.
(28) Schniepp, H. C.; Li, J. L.; Mcallister, M. J.; Sai, H.; Alonso, M. H.; Adamson, D. H.; Prudhomme, R. K.; Car, R.; Saville, D. A.; Aksay, I. A. *J. Phys. Chem. B.* **2006**, *110*, 8535−8539.
(29) Fang, M.; Zhang, Z.; Li, J.; Zhang, H.; Lu, H.; Yang, Y. *J. Mater. Chem.* **2010**, *20*, 9635−9643.
(30) Chen, D.; Zhu, H.; Liu, T. *ACS Appl. Mater. Interfaces* **2010**, *2*, 3702−3708.
(31) Park, O.-K.; Hahm, M. G.; Lee, S.; Joh, H.-I.; Na, S.-I.; Vajtai, R.; Lee, J. H.; Ku, B.-C.; Ajayan, P. M. *Nano Lett.* **2012**, *12*, 1789−1793.
(32) Lai, L.; Chen, L.; Zhan, D.; Sun, L.; Liu, J.; Lim, S. H.; Poh, C. K.; Shen, A.; Lin, J. *Carbon* **2011**, *49*, 3250−3257.
(33) Bolotin, K. I.; Siles, K. J.; Jing, M.; Klima, G.; Fudenberg, G.; Hone, J.; Kim, P.; Stomer, H. L. *Solid. State. Commun.* **2008**, *146*, 351−355.
(34) Chen, J. H.; Jang, C.; Xiao, S.; Ishigami, M.; Fuhrer, M. S. *Nat. Nanotechnol.* **2008**, *3*, 206−209.
(35) Balogun, Y. A.; Buchanan, R. C. *Compos. Sci. Technol.* **2010**, *70*, 892−900.
(36) Yousefi, N.; Gudarzi, M. M.; Zheng, Q.; Aboutalebi, S. H.; Sharif, F.; Kim, J.-K. *J. Mater. Chem.* **2012**, *22*, 12709−12717.
(37) Ezquerra, T. A.; Kulescza, M.; Cruz, C. S.; Balta-Calleja, F. J. *Adv. Mater.* **1990**, *2*, 597−600.
(38) Ku, B. C.; Blumstein, A.; Kumar, J.; Samuelson, A.; Kim, D. W. *Dekker Encycl. Nanosci. Technol.* **2004**, *1*, 213−225.
(39) Tsai, M.-H.; Tseng, I.-H.; Liao, Y.-F.; Chiang, J.-C. *Polym. Int.* **2012**, *53*, 1479−1484.
(40) Nair, R. R.; Wu, H. A.; Jayaram, P. N.; Grigorieva, I. V.; Geim, A. K. *Science* **2012**, *335*, 442−444.
(41) Huang, H.-D.; Ren, P.-G.; Chen, J.; Zhang, W.-Q.; Ji, X.; Li, Z.-M. *J. Membr. Sci.* **2012**, *409−410*, 156−163.